American Mineralogist, Volume 60, pages 351–358, 1975

Multiple Beam Direct Lattice Imaging of New Mixed-Layer Compounds of the Bastnaesite-Synchisite Series[1]

J. Van Landuyt, and S. Amelinckx[2]

Rijksuniversitair Centrum Antwerpen,
Middelheimlaan, 1, B-2020 Antwerpen, Belgium

Abstract

Electron microscopy and diffraction techniques have been used for studying the mixed-layer compounds in the bastnaesite-synchisite series. Using multiple beam direct lattice imaging, the elementary building blocks of these minerals could be imaged. An imaging code was established experimentally from the analysis of characterized species from the series.

Intimate syntaxy between parisite, synchisite, roentgenite, and bastnaesite was quite commonly observed even on a very fine scale. Lattice imaging and electron diffraction enabled us to identify three new compounds within the bastnaesite-synchisite series. Irregular sequences of layers as observed by this technique readily explain the "disordered species" detected previously by X-ray diffraction. Optical simulation of the electron-diffraction patterns substantiates the layer model for the new compounds.

Introduction

Direct lattice resolution in transmission electron microscopy has become a powerful tool for the study of mixed-layer polytypes (Van Landuyt, Amelinckx, Kohn, and Eckart, 1973, 1974) and long period complex oxides (Cowley and Iijima, 1972; Allpress, Hewat, Moodie, and Sanders, 1972). The different stacking modes of the constituent layers can be made directly visible. Also, structures with a very large repeat distance, which can only be studied with considerable difficulty by means of X-ray diffraction, can be observed with relative ease by means of electron microscopy. Even irregular sequences can be imaged directly.

The application of direct lattice resolution to minerals has as yet been limited (Buseck and Iijima, 1974; Van der Sande and Kohlstedt, 1974); in the present paper we demonstrate its application to the study of the mixed-layer compounds of the bastnaesite-synchisite type.

Structure in the Bastnaesite-Synchisite Series

According to Donnay and Donnay (1953) "single" crystals of the minerals of this type may in fact consist of components of different mineral species. Donnay and Donnay proposed the name "polycrystal" for these intergrowths. These intergrowths are composed of species such as bastnaesite $LnFCO_3$, parisite $2LnFCO_3 \cdot CaCO_3$, roentgenite $3LnFCO_3 \cdot 2CaCO_3$, and synchisite $LnFCO_3 \cdot CaCO_3$. Parisite and roentgenite can be considered as containing layers of bastnaesite and synchisite in varying proportions (Caro, 1973). Except for bastnaesite (Donnay and Donnay, 1953), a detailed structure determination has not been possible because X-ray diffraction experiments always reveal a considerable degree of disorder. Striking, direct evidence for the nature of the "disorder" will be illustrated in this paper.

The structure of this family of minerals has been described qualitatively in terms of four different types of layers parallel to the hexagonal (0001) plane by Donnay and Donnay (1953).

(d) LnF ionic layers
(e) layers of Ca ions
(f) layers of CO_3 groups between two LnF layers
(g) layers of CO_3 groups between a calcium- and a LnF layer.

With these notations one can represent the different structures by means of the layer sequences of Table 1 and by means of Figure 1 where the CO_3 groups between LnF layers are marked by vertical hatching. These lines are related to the inclination of the plane of the CO_3 groups.

[1] Work performed under the auspices of the association RUCA-SCK.

[2] Also at SCK-CEN, Mol (Belgium).

TABLE 1. Layer Sequences, Spacing, and Block Symbols for the Bastnaesite–Synchisite Series

Mineral	Layer Sequence	Spacing	Block Symbol
Bastnaesite	de/de/...	9.7 Å	B
Parisite	dedgfg/dedgfg/...	23.14 Å (x3?)	BS
Roentgenite	dedgfgdgfg/dedgfgdgfg/...	28.04 Å (x3?)	BS_2
Synchisite	dgfg/dgfg/...	18.24 Å (x3?)	S

Another description can be given in terms of blocks *de* of bastnaesite (B) and blocks *dgfg* of synchisite (S), which can be considered the two end members of the series. The corresponding symbols are also given in Table 1.

It is reasonable to expect that more sequences corresponding to various proportions of bastnaesite and synchisite layers are possible, and in fact we shall present evidence that this is indeed the case. Until now, however, the four mentioned minerals are the only ones known to occur in nature.

Experimental

Origin of the Material

The material consisted of small brownish intergrown crystals from Narsarsuk, Greenland, that were placed at our disposal by the Belgian Institute of Natural History, Brussels. The material used by Donnay and Donnay (1953) came from the same locality.

Specimen Preparation

Since the main interest lies in ascertaining block sequences by means of lattice resolution, very thin specimens are needed, with the foil plane roughly perpendicular to the set of planes that limits the blocks to be resolved. The simplest method for preparing such specimens consists in grinding the crystals and dispersing the fragments in alcohol on thin perforated carbon films. Because of the small size of the "polycrystals" (~0.2 mm), this is the only practical method. No pronounced basal cleavage seems to occur, which is a favorable feature for the present application. The fragments can be oriented with the goniometer stage into the required orientation. The most suitable specimens are those which partly cover a hole in the supporting film; the part of the crystal that projects over the hole is the part to be examined.

Observation Techniques

With the goniometer stage the specimens are brought into an orientation such that the electron beam is exactly parallel to (0001). This can most easily be achieved by operating the electron microscope in the diffraction mode and tilting the crystal during observation until a systematic row of closely spaced spots of the type *000l* becomes visible over its whole length. In some cases the crystal is oriented so that a complete reciprocal lattice plane is excited. We made both bright field (B.F.) and dark field (D.F.) images using *000l* spots of the central row or spots of a non-central row. The aperture is chosen to admit at least three main spots, *i.e.*, spots corresponding to a spacing of approximately 14 Å.

Lattice fringes have a contrast that changes with the local foil orientation, with the foil thickness, and with the amount of focussing of the microscope. In dark field conditions, the best contrast is found in those areas where bright contours extend into the thinnest part of the specimen, close to the edges. In order to obtain comparable images of the different mixed-layer structures, the same set of main spots was always selected using the same aperture. Such line images (Fig. 2) are comparable with those obtained from hexagonal ferrites (Van Landuyt *et al,* 1974).

Some images were made using non-central row reflections (*e.g.*, Fig. 3). It is shown there that such images may contain more information than central-row dark-field images or than bright-field images, because they reveal possible twinning on the (0001) plane (Van Landuyt *et al,* 1974).

Observed Spacings, Imaging Code

A number of different line spacings, observed even in crystal fragments originating from the same "crystal," showed that different stacking sequences are present in the same macroscopic specimen.

The selected area diffraction patterns reveal different spacings, which in all cases are correlated

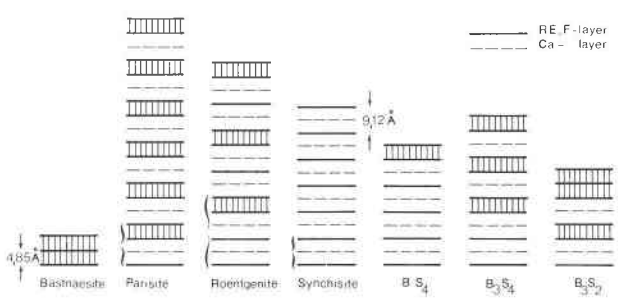

FIG. 1. Schematic representation of different mixed-layer compounds in the series bastnaesite-synchisite (after Donnay and Donnay, 1953). Possible models for the new compounds are also shown. For the new compounds only one period of the layer sequence is illustrated; the vertical hatching is related to the plane of the CO_3 layers.

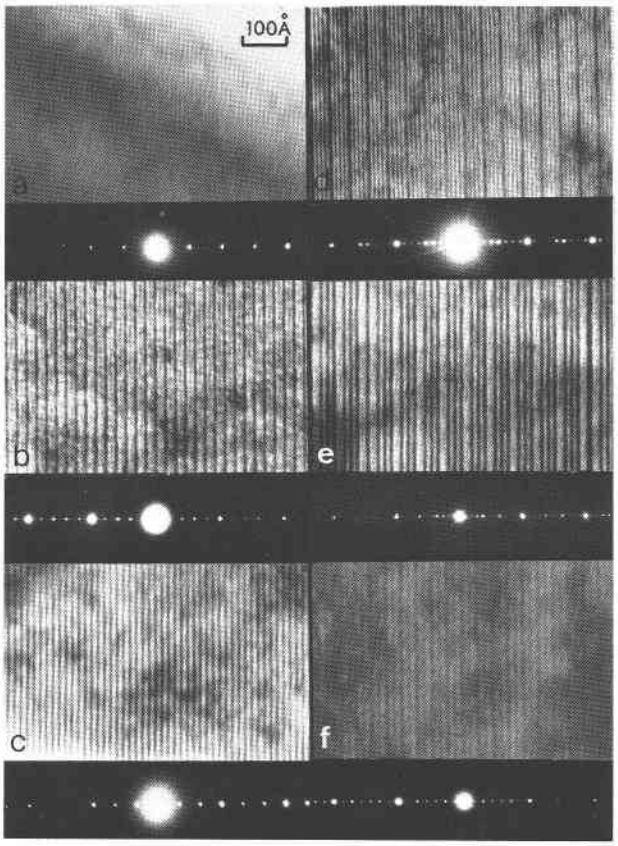

FIG. 2. Line images and corresponding [000*l*]* row on the diffraction pattern: (a) S (synchisite), (b) BS_2 (roentgenite), (c) BS (parisite), (d) BS_4, (e) B_3S_4, (f) B_3S_2. In the case of bastnaesite, no lattice fringes are resolved. All photographs and diffraction patterns are at the same magnification.

with the line spacings of the images, proving that the latter reveal the lattice.

Two main types of line patterns and corresponding diffraction patterns were distinguished initially, corresponding to roentgenite (Fig. 2b) and parisite (Fig. 2c). The spacings are respectively 23 Å and 14 Å, as derived from the image and from the diffraction pattern; these spacings correspond with those determined by means of X-ray diffraction for roentgenite and parisite, enabling identification of the two compounds and establishment of the imaging code.

Parisite (Fig. 2c) is imaged by means of equally spaced identical heavy lines with a spacing of 14 Å, whereas roentgenite is represented as a sequence of lines of two types, one being heavier than the other (Figs. 2b, 4a) or, under other diffraction or thickness conditions, by means of lines having alternately a larger and a smaller spacing (Fig. 4b). The repeat distance in each case is 23 Å. Noting that a bastnaesite layer has a thickness of 4.85 Å and a synchisite layer a thickness of 9.12 Å, one obtains a consistent imaging code for parisite and roentgenite when ascribing the larger interline spacing of 14 Å in the image to a BS layer and the smaller interline spacing of 9 Å to an S layer.

It is well known that, in sufficiently thin foils and under conditions of slight underfocussing, the bright field image is closely related to the projected charge density (Cowley and Iijima, 1972). With this in mind the alternating heavy and weak lines in roentgenite can be interpreted as being related respectively to the double layer . . . *ded* . . . and the single layer . . . *gdg* . . . of heavy rare earth layers *d*. This turns out to be true for the dark field as well as for the bright field image. In the structure models in Figure 1, the hatched bands are imaged as a heavy line, the full lines are visible as a faint line, whereas the dashed lines, corresponding to the calcium layers, are not resolved. The correspondence between the two imaging codes is shown in Figure 4, where a weak line in one of the images corresponds with a small interline spacing in the other, and a heavy line with a large interline spacing. Matching of the two types of images is easily done by using defects in the stacking as indicated by arrows in Figure 4 c and d.

Transition from one imaging code to the other may result from changes in thickness near the edge of the specimen, changes in orientation of the foil, or differences in focussing conditions. Similar correspondences were noted previously in the case of the hexagonal ferrites (Van Landuyt *et al,* 1974).

It should be emphasized that the primary imaging code, *i.e.,* the one observed in the thinnest sections and at slight underfocussing is the most reliable for direct identification since, as stated by Cowley and Iijima (1972), these images have the closest relation with the charge density. The second imaging code is in fact the reverse contrast which should be inter-

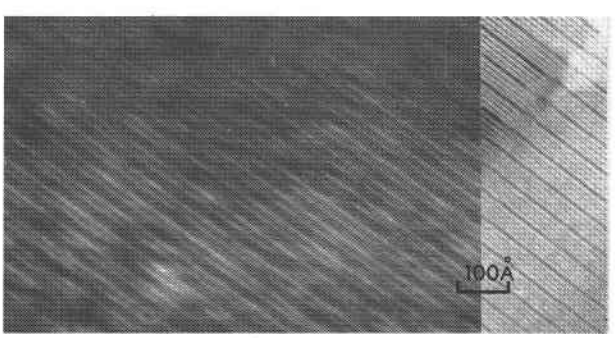

FIG. 3. Non-central-row dark-field image revealing "twinning" on unit-cell scale in BS_4. As inset a central-row line image of the same specimen is matched to illustrate the correspondence.

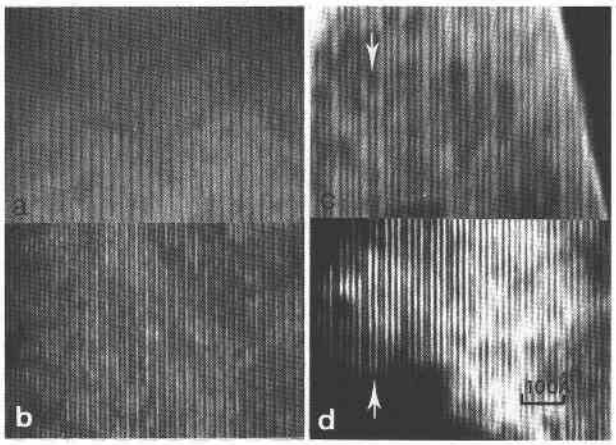

FIG. 4. Correspondence between the two imaging codes: (a) and (b) roentgenite; (c) and (d) B_3S_4.

preted with the necessary care. It is mentioned here because it often appears in the same images. The other imaging situations can be used provided these are calibrated against known structures. This is the justification of the procedure used in the present paper.

New Compounds

a) *Lattice Images*

Having established the imaging code, we looked for new stacking sequences and discovered three hitherto unreported mixed-layer compounds of the type B_mS_n. We consider a stacking sequence to correspond to a different compound if it produces a well-defined diffraction pattern and a line image exhibiting regions containing at least ten identical repeat sequences. Moreover, we require the same repeat to occur at least in three different crystal fragments. The line images of the new compounds are shown (Fig. 2, d, e, f) together with the corresponding diffraction patterns.

According to the imaging code deduced in the previous paragraph, the block symbols for these compounds are: BS_4, B_3S_4, and B_3S_2. Taking into account the thicknesses of the B and S layers, the repeat distances given in Table 2 correspond to those measured on the line images and to those derived from the diffraction patterns. This proves that the model is consistent with the line images as well as with the diffraction patterns. A structure model for these new compounds is included in Figure 1. Only one period of the stacking sequence is shown.

TABLE 2. Compositions for the Bastnaesite–Synchisite Series

Block Symbol	Composition	d_{0001}
BS_4	$(CeFCO_3)_5(CaCO_3)_4$	41.92 Å
B_3S_4	$(CeFCO_3)_7(CaCO_3)_4$	51.03 Å
B_3S_2	$(CeFCO_3)_5(CaCO_3)_2$	32.79 Å

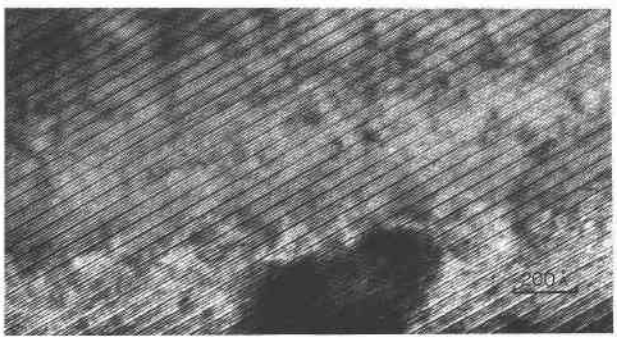

FIG. 5. Large region of faultless BS_4 (both imaging codes are visible).

Figure 5 shows a large region of faultless BS_4. In this dark field image, the line pattern close to the edge of the specimen (the lower part of Fig. 5) reveals one BS spacing followed by three S spacings. In another region (top part, Fig. 5), where the other imaging code is valid, one notes a regular succession of three weak lines and a strong line.

The sequence in Figure 2e corresponds to a composition close to that of parisite since its block sequence is B_3S_4; *i.e.*, three BS blocks alternate with one S block. In the dark field image of Figure 6, the two imaging codes are present simultaneously. Close to the edge is a regular succession of three large and one small interline spacing. For larger thicknesses the im-

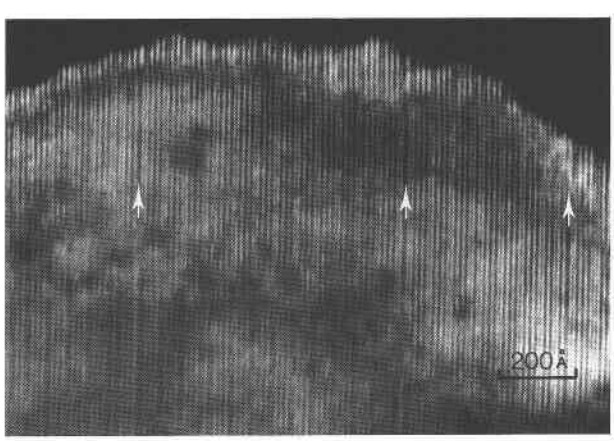

FIG. 6. Large region of B_3S_4; the two imaging codes are present simultaneously.

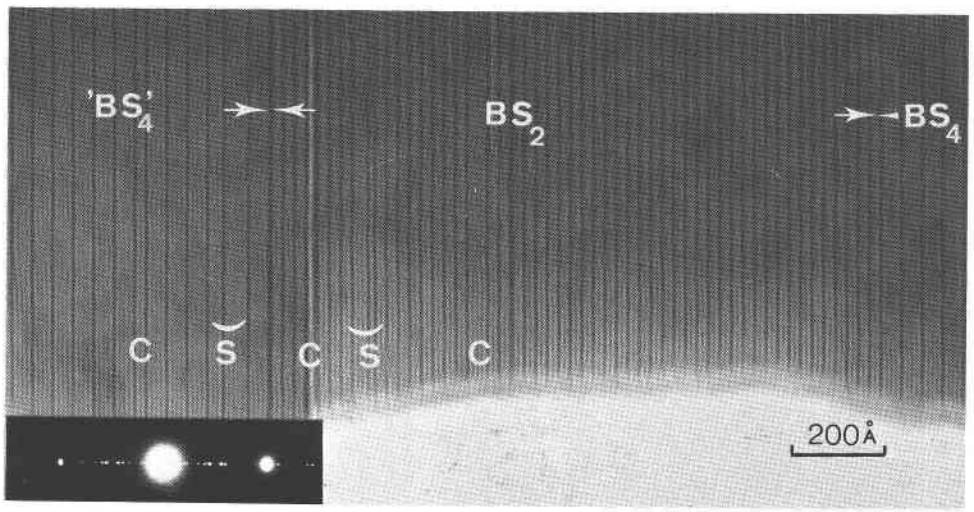

FIG. 7. Example of syntaxy. A nearly perfect roentgenite region has grown between two BS_4 regions. Stacking sequences marked S and C correspond respectively to sequential and compositional faults.

age consists of a regular succession of three heavy lines and a weak line. In still thicker parts the two different spacings appear again. In the bright field image, the same type of line sequence is found in the thin parts, confirming the model. Figures 4 c and d clearly illustrate the correspondence between the two imaging codes. Note also some faults in the stacking sequence marked by closely spaced heavier lines in Figure 6; these are presumably successive unresolved B blocks.

"Sequential faults," as defined by Van Landuyt *et al* (1974), have also been observed. An example is shown at S in Figure 7. At these faults the succession of layers is wrong but the composition remains unchanged.

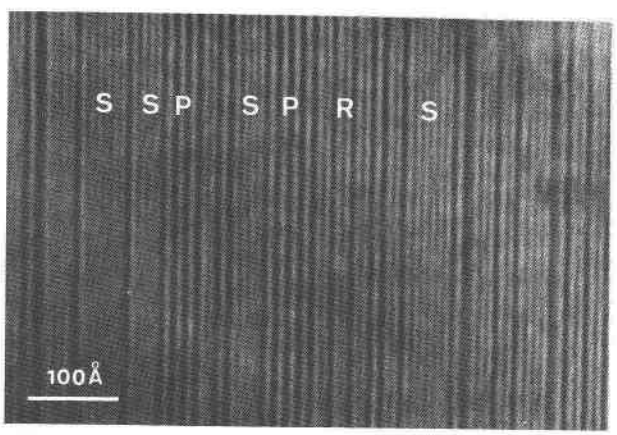

FIG. 8. Typical example of microsyntaxy in a "polycrystal" diffracting as a disordered phase. Narrow regions (~100 Å) of parisite (P), roentgenite (R), and synchisite (S) are randomly intergrown.

Fine Scale Syntaxy. From the electron microscope images, it becomes evident that syntaxic intergrowth also occurs on a fine scale. Adjacent parts of the same crystalline fragment may present different sequences. In Figure 7, for instance, a band

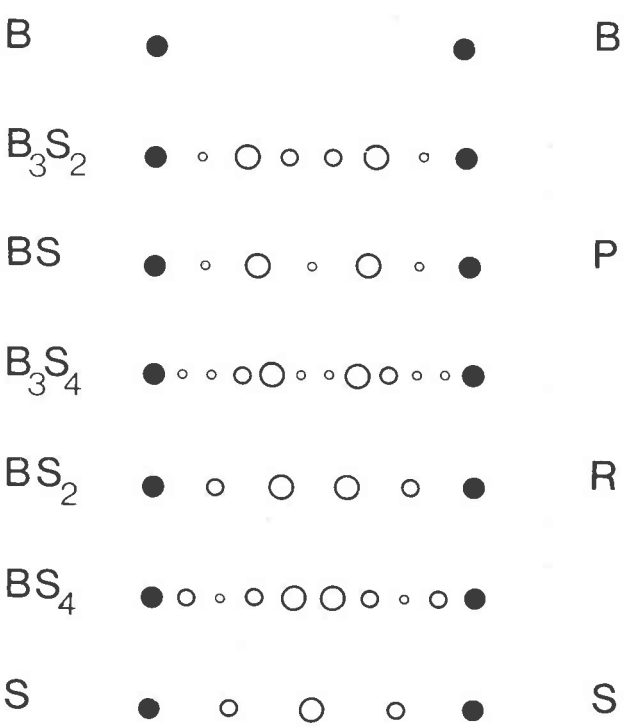

FIG. 9. Schematic representation of the [000*l*]* rows of the diffraction patterns due to the different mixed-layer compounds. The relative size of the circlets is a rough measure of the relative intensities. The pseudo-period c'''(Donnay and Donnay, 1953) corresponds to the filled circlets in the row.

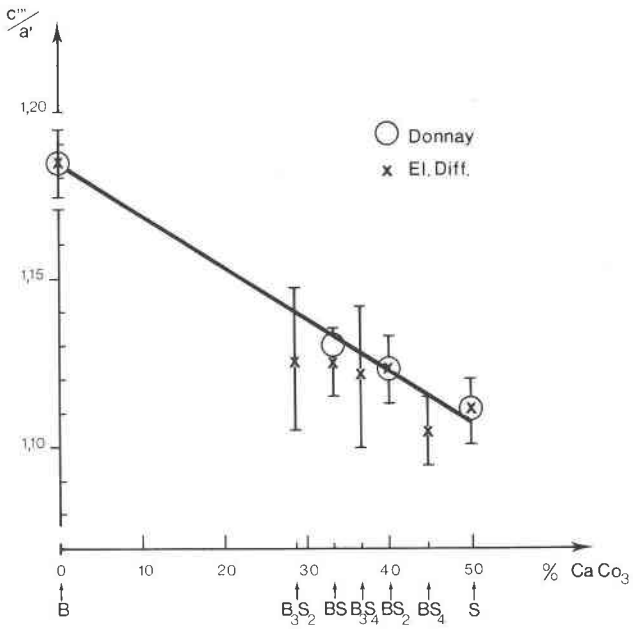

FIG. 10. The ratio c'''/a' (notation of Donnay and Donnay) plotted as a function of composition. Circlets show values obtained by X-ray diffraction (Donnay and Donnay, 1953); crosses with error bars give electron-diffraction results (present paper).

of roentgenite is enclosed between two regions of the new type BS_4. Both regions contain occasional faults. The diffraction pattern (inset) results from the superposition of the diffraction patterns due to the two sequences. Figure 8 gives a particular example of microsyntaxy: layers of parisite (P), roentgenite (R), and synchisite (S) with a thickness of only ~100 Å are intergrown in perfect syntaxy.

Irregular Sequences. X-ray diffraction experiments have demonstrated that these compounds are often disordered (Donnay and Donnay, 1953). Many of the observed line patterns indeed reveal compositional faults, which may or may not be associated with stacking faults. A compositional fault can easily be detected as a pair of lines with an abnormal spacing. Such faults are visible in Figure 7, where they are labelled C. The large variety of irregular sequences observed by the present techniques clearly explains "the disordered species" that were detected by X-ray diffraction, and the resultant difficulties encountered in determining accurate lattice parameters and other physical constants such as the indices of refraction (Donnay and Donnay, 1953).

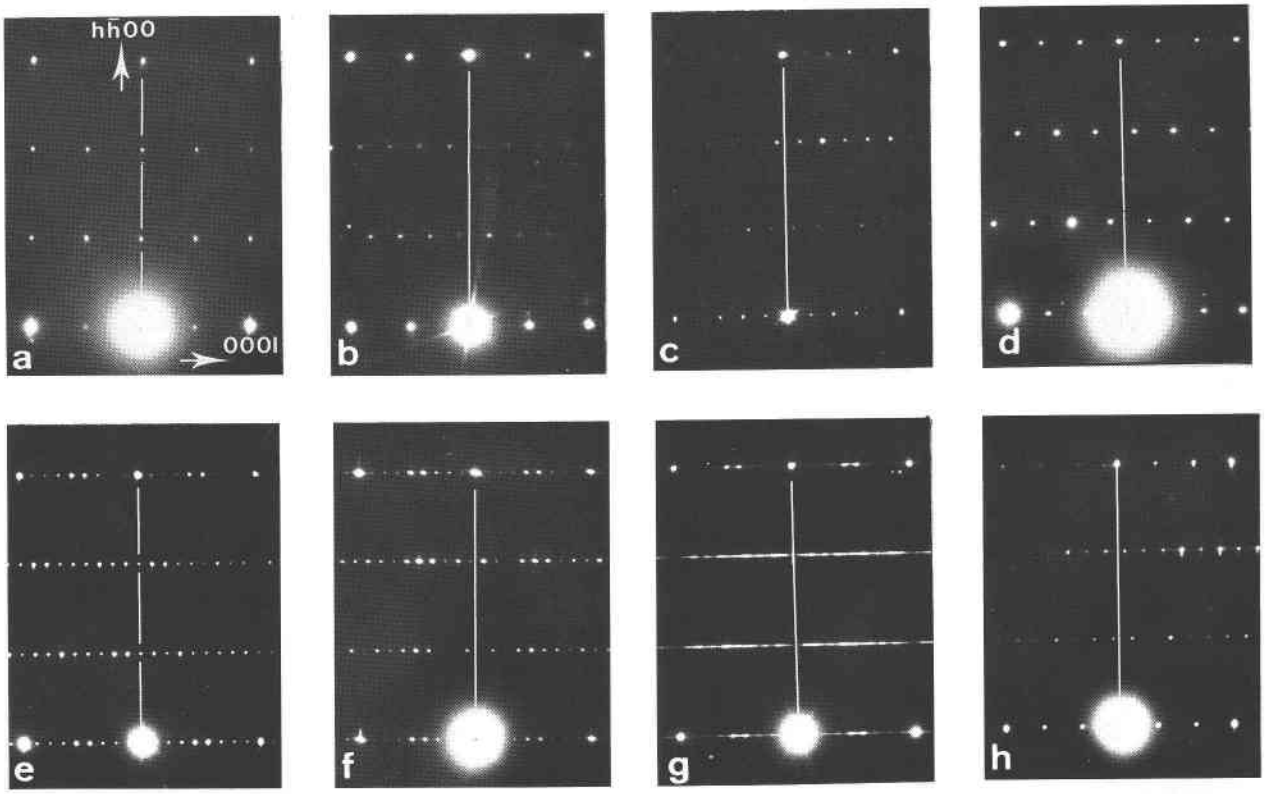

FIG. 11. Two-dimensional sections through the reciprocal lattice of different compounds. (a) B: bastnaesite (hexagonal); (b) S: synchisite; (c) BS_2: roentgenite; (d) BS: parisite (rhombohedral, c = 14 Å); (e) BS_4: hexagonal; (f) BS_4: rhombohedral; (g) BS_4: faulted; (h) BS: parisite rhombohedral, c = 28 Å). Vertical lines help distinguish hexagonal (a) and (e) from rhombohedral forms.

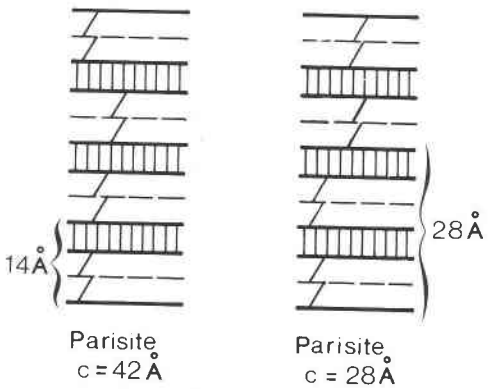

FIG. 12. Structural models for the two polytypes of parisite. The inclined lines between the Ca and Rare Earth layers (R.E.) are related to the inclination of the plane of the CO_3 group.

b) *Electron-Diffraction Data*

The electron-diffraction patterns (Fig. 2) can be compared directly with the X-ray diffraction patterns published by Donnay and Donnay (1953, their Fig. 2). The simplest procedure is to look in the c^* direction for the spots corresponding to the most prominent pseudo-period. In bastnaesite such spots correspond to d_{0002} ~4.9 Å, half the true c repeat. In synchisite the pseudo-period is d_{0004} ~4.6 Å, as shown by the three weak spots between strong spots (Fig. 2a). In roentgenite there are four weak spots between strong spots so that the pseudo-period is $d_{0005} = c/5$ (Fig. 2b). Finally in parisite five weak spots are observed (Fig. 2c) which lead to $d_{0006} = c/6$. Figure 2 also shows the diffraction patterns of the new compounds. The diffraction patterns can clearly be used to identify the known compounds and also to "calibrate," in a sense, the corresponding images in terms of block sequences. The characteristic aspects of the $[000l]^*$ row of the diffraction patterns are reproduced schematically in Figure 9.

We confirm, at least qualitatively, the systematic variation of the pseudo-period c''' with composition as described by Donnay and Donnay (1953). In order to compare our measurements with those of Donnay and Donnay, we plotted the c'''/a' ratio (Fig. 10) for all seven compounds from bastnaesite to synchisite. The circlets are the values given by Donnay and Donnay; the crosses with error bars are our measurements. The systematic variation with composition is qualitatively well confirmed.

We found a considerable variation of the c'''/a' ratio from specimen to specimen; this may be because the stacking sequence is not perfect. The new compounds fit satisfactorily into this scheme. For B_3S_2 and B_3S_4 only a few measurements of the c''' spacing were available. The lack of internal calibration, by measurement of the a' spacing on the same film, results in a larger error.

A complete set of two-dimensional sections (110)* (Fig. 11) shows the reciprocal period c^* for each compound and presents evidence for the hexagonal or rhombohedral character of each lattice. It can be concluded from Fig. 11, d and h, that parisite occurs in two rhombohedral polytypes with, respectively, 14 Å and 28 Å as basic repeats. A model is shown in Figure 12.

From the BS_4 patterns we deduce that this new compound also occurs in two polytypes, with the same chemical composition but with a different stacking sequence; one is hexagonal (Fig. 11e), the other rhombohedral (Fig. 11f). In the latter successive c^* rows are shifted over 1/3 of the c^* period; as a result the pattern is not orthogonal like the hexagonal polytype.

On the non-central-row, dark-field image of hex-

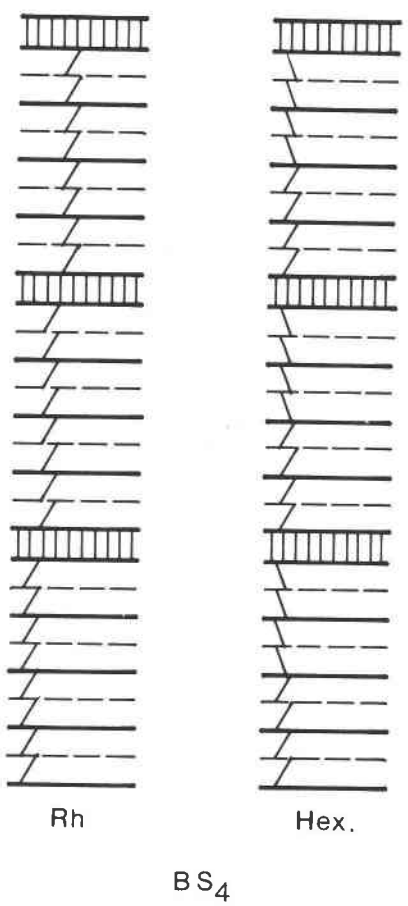

FIG. 13. Polytypes of BS_4: (a) rhombohedral modification; (b) hexagonal modification. The twinning as indicated by the inclination of the lines is related to the occurrence of the polytypes.

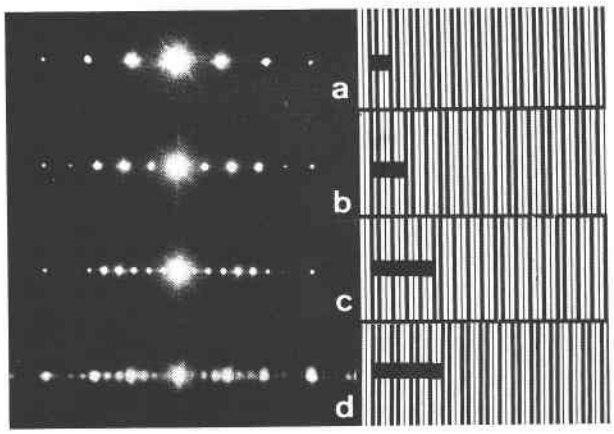

FIG. 14. Optical simulation of the diffraction patterns. The line patterns are juxtaposed to the diffraction patterns. The thick bars indicate the repeat distance. (a) parisite: BS; (b) roentgenite: BS_2; (c) BS_4; (d) B_3S_4.

agonal BS_4 (Fig. 3), successive pairs of synchisite slabs exhibit different contrasts. This observation strongly suggests that the four-layer synchisite blocks are in fact internally "twinned," as shown schematically in Figure 13.

Owing to compositional or sequential disorder, some crystal fragments have only an average composition. The area marked "BS_4" (Fig. 7) has the BS_4 composition only on the average. The diffraction pattern corresponding to such a situation (Fig. 11g) shows that, as a result of this type of disorder, the superlattice spots have vanished, except for the two spots near the middle of the repeat that correspond to the basic spacing.

Optical Simulation of the Diffraction Patterns

In order to confirm the proposed structure, we compared the intensity variation of the diffraction spots in the [000*l*]* rows of the electron-diffraction patterns with optical diffraction patterns of one-dimensional models. The optical diffraction patterns and the optical masks respectively used to simulate parisite (a), roentgenite (b), BS_4 (c), and B_3S_4 (d) (Fig. 14, a, b, c, d) are to be compared with the electron-diffraction patterns and corresponding line images (Fig. 2, c, b, d, e, respectively, and Fig. 9). Apart from a more rapid decrease of the spot intensities from the center outwards in the optical patterns, the resemblance is striking as regards the relative intensities of the diffraction spots.

Acknowledgments

Thanks are due to Professor R. Van Tassel, Curator of the Mineralogy Department of the "Royal Belgian Institute for Natural History," Brussels, for providing us with some parisite crystals from the National Collection.

References

ALLPRESS, J. G., E. A. HEWAT, A. F. MOODIE, AND J. V. SANDERS (1972) *n*-beam lattice images, Part I. *Acta Crystallogr.* **A28,** 528–536.

BUSECK, P. R., AND S. IIJIMA (1974) High resolution electron microscopy of silicates. *Am. Mineral.* **59,** 1–21.

CARO, P. E. (1973) Structures lamellaires: Syntaxie, polytypie et non-stoechiométrie. *J. Solid State Chem.* **6,** 396–401.

COWLEY, J. M., AND S. IIJIMA (1972) Electron microscope image contrast for thin crystals *Z. Naturforsch.* **27a,** 445–451.

DONNAY, G., AND J. D. H. DONNAY (1953) The crystallography of bastnaesite, parisite, roentgenite, and synchisite. *Am. Mineral.* **38,** 932–963.

VAN DER SANDE, J. B., AND D. L. KOHLSTEDT (1974) A high resolution electron microscopy study of exsolution lamellae in enstatite. *Phil. Mag.* **29,** 1041–1049.

VAN LANDUYT, J., S. AMELINCKX, J. A. KOHN, AND D. W. ECKART (1973) Lattice imaging of the hexagonal ferrites: The M_n S-series. *Mat. Res. Bull.* **8,** 1173–1182.

———, ———, ———, AND ——— (1974) Multiple beam direct lattice imaging of the hexagonal ferrites. *J. Solid State Chem.* **9,** 103–119.

Manuscript received, August 22, 1974; accepted for publication, December 17, 1974.